A coupled modal-finite element method for the wave propagation modeling in irregular open waveguides

Adrien Pelat, Simon Félix, Vincent Pagneux

A coupled Modal - Finite Element method for the wave propagation modeling in irregular open waveguides

Adrien Pelat,[a] Simon Félix, and Vincent Pagneux
LAUM, CNRS, Université du Maine, avenue Olivier Messiaen, 72085 Le Mans, France.

In modeling the wave propagation within a street canyon, a particular attention must be paid to the description of both the multiple reflections of the wave on the building façades, and the radiation in the free space above the street. The street canyon being considered as an open waveguide with a discontinuously varying cross-section, a coupled modal-FE formulation is proposed to solve the three-dimensional wave equation within. The originally open configuration - the street canyon open in the sky above - is artificially turned into a close waveguiding structure by using Perfectly Matched Layers (PML) that truncate the infinite sky without introducing numerical reflection. Then the eigenmodes of the resulting waveguide are determined by a FEM computation in the cross-section. The eigensolutions can finally be used in a multimodal formulation of the wave propagation along the canyon, given its geometry and the end conditions at its extremities : initial field condition at the entrance and radiation condition at the output.

PACS numbers: 43.28.Js,43.20.Mv

I. INTRODUCTION

As a medium of sound propagation, the center of urban areas consists of interconnected confined spaces - the street canyons - in which the sound is both confined (the space is enclosed by buildings) and radiated into free space (the canyon is open on the sky above). In modeling the sound propagation within a street canyon, the effects of the open ceiling must be taken into account. In the high frequency approximation the height of the canyon is either assumed as infinite[9,10,12] or, equivalently, the opening at the top is represented by a perfectly absorptive ceiling[11]. At lower frequencies, the effect of the finite height of the streets and the radiation of sound above is considered in[6,13,17]. However, these works are restricted to solutions of the two-dimensional wave equation in the plane of the canyons cross-sections. Hornikx and Forssén recently extended these results to solve the 3D wave equation, in the case of infinite, uniform, canyons[7]. It is the aim of the present study to take into account the effect of both the finite height of the street and the non-uniformities of the buildings enclosing the canyon.

We consider the sound propagation in an open waveguide as an idealized model of a street canyon. In such a geometry, and more generally when the wave is not totally confined by the guiding geometry or medium (we can refer to other wave types as elastic waves in embedded waveguide[3] or electromagnetic waves in optical fiber[18]), the modes of the waveguide become *leaky*, owing to the radiative losses in the infinite space - the sky over the street in the context of urban noise. In a previous paper by the authors, it was shown how the leaky modes can be used as a basis for a multimodal formulation of the sound propagation within the open waveguide[15]. The modes of the waveguide were calculated by first deriving the dispersion relation for the frequencies of the resonances in a rectangular cavity open in an infinite halfspace. Then, this dispersion relation was solved numerically to give a set of eigenfrequencies and eigenfunctions used for the mutimodal formulation of the sound propagation. As detailed below, note that in this study, the eigenmodes are obtained using the Finite Elements Method (FEM).

Although this preliminary study[15] suited its aim - determining the leaky modes and their properties, and showing, notably, how a limited number of these modes can be sufficient to accurately model the wave field - it might prove inadequate when considering more complex problems, as varying cross-section waveguides because of the non-straightforward mode matching at each cross-sectional change.

Since the Perfectly Matched Layers[1] (PML) enable to efficiently truncate an open, infinite domain to design a computational domain of finite dimensions, an alternative approach to[15] is to turn the originally open waveguide into a closed waveguiding geometry. Then the modes of the resulting closed waveguide can be used for a modal formulation of the wave propagation[4]. The modal-FE method, developed in the following paper, consists, first, in deriving the eigenmodes using a finite elements discretization of the cross-section. Then, an impedance matrix formulation, similar to the one extensively studied in "classical" waveguides[2,5,14], is used to write the wave propagation along the waveguide, given the input and output conditions at the ends of the domain of interest.

II. 2D PRELIMINARY STUDY: WAVE PROPAGATION IN A SEMI-INFINITE HALFSPACE

In order to clearly describe the principles of the modal-FE method for modeling the wave propagation in partially bounded elongated domains, the 2D case of the propagation over an infinite ground is first considered and analyzed in this section. In this simple case, analytical solutions can be used to validate the method. Let

[a] Electronic address: adrien.pelat@univ-lemans.fr

the ground be defined by $z =$ constant, z the vertical coordinate (the case of a ground with a piecewise constant, range dependent, height, is considered later in the paper). Over this boundary that is assumed to be perfectly reflecting, one whishes to solve the wave equation

$$\left(\nabla^2 + k^2\right) p = 0, \tag{1}$$

with $k = \omega/c_0$ the wavenumber and c_0 the wave speed, together with end conditions at the extremities of the region of interest, say, $x = 0$ and $x = L$, x the range coordinate (time dependence $\exp(-\mathrm{j}\omega t)$ is omitted).

This problem in an open domain is now substituted by the new problem of a bounded elongated domain, by introducing a PML of finite width h in the z-direction, with an homogenous Neumann condition at the end (Fig. 1(a)). Eq. (1) becomes

$$\left[\frac{\partial^2}{\partial x^2} + \frac{1}{\tau}\frac{\partial}{\partial z}\left(\frac{1}{\tau}\frac{\partial}{\partial z}\right) + k^2\right] p(x,z) = 0, \tag{2}$$

with $\tau(z)$ a complex scalar parameter fulfilling

$$\begin{cases} \tau = \tau_0 & \text{if } z > 0, \\ \tau = 1 & \text{if } z \leq 0 \end{cases} \tag{3}$$

(see details in App. A). In the sequel, it is chosen $\tau_0 =$ constant $= A\exp(\mathrm{j}\beta)$, with $A > 0$ and $\beta \in]0, \pi/2[$ so that $\Re\{\tau_0\}\Im\{\tau_0\} > 0$.

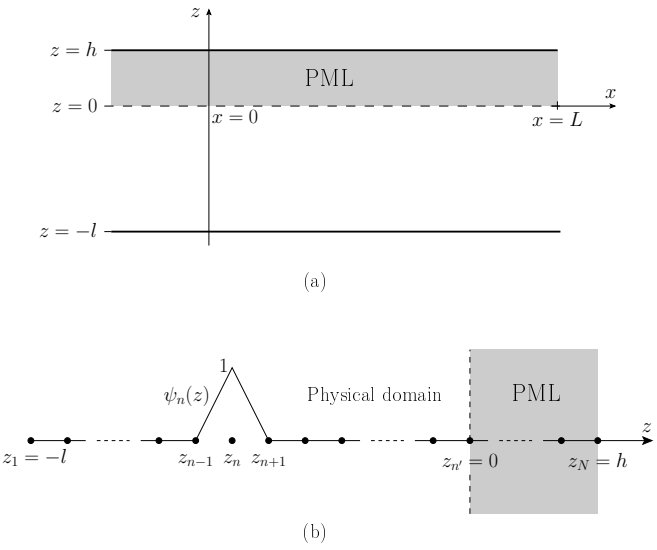

Figure 1. (a) The halfspace above a perfectly reflecting flat boundary is represented by a 2D waveguide closed by a PML. (b) The 1D cross-section is discretized on a N-nodes grid. A first order interpolating polynomial $\psi_n(z)$ corresponds to each element n.

Then, the cross-section $z \in [-l, h]$ is discretized on a N-nodes grid: $-l = z_1 < z_2 < \ldots < z_{n'} = 0 < \ldots < z_N = h$ (Fig. 1(b)), and the pressure field is developed on a basis of first order interpolating polynomials $\psi_n(z)$:

$$p(x,z) = \sum_{n\geq 1} P_n(x)\psi_n(z) = {}^{\mathrm{t}}\vec{\psi}\vec{P}, \tag{4}$$

where the components of $\vec{P}$ are the values of the pressure at nodes z_n: $P_n(x) = p(x, z_n)$. Following the development (4), Eq. (2) is reformulated as

$$\vec{P}'' + \left(M^{-1}K + k^2\right)\vec{P} = 0, \tag{5}$$

where $''$ denotes the second derivative with respect to x, and mass and stiffness matrices M and K are given by, respectively,

$$M_{mn} = \int_{-l}^{h} \tau\psi_m\psi_n \,\mathrm{d}z, \tag{6a}$$

$$K_{mn} = -\int_{-l}^{h} \frac{1}{\tau}\frac{\partial\psi_m}{\partial z}\frac{\partial\psi_n}{\partial z}\,\mathrm{d}z. \tag{6b}$$

A general solution of Eq. (5) can be written as function of the eigenvalues α_i^2, $i \geq 0$, and eigenfunctions ϕ_i of the matrix $M^{-1}K$:

$$\vec{P} = \Phi\left(D(x)\vec{C_1} + D(L-x)\vec{C_2}\right), \tag{7}$$

where $\Phi = [\phi_0, \phi_1, \phi_2, \ldots]$ and $D(x)$ is a diagonal matrix given by

$$D_i(x) = e^{\mathrm{j}k_i x}, \tag{8}$$

with $k_i = \sqrt{k^2 - \alpha_i^2}$ ($\Re\{k_i\} \geq 0$, $\Im\{k_i\} \geq 0$). $\vec{C_1}$ and $\vec{C_2}$ are constant vectors determined by the end conditions at $x = 0$ and $x = L$. Let assume that the condition at $x = 0$ is defined as a given pressure field $\vec{P_0}$ and the condition at $x = L$ as an admittance matrix Y_L fulfilling $\vec{Q}(L) = Y_L\vec{P}(L)$, with $\vec{Q}$ the vector of the components of $\partial_x p$ in the basis $\{\psi_n\}$. Then, the constants $\vec{C_1}$ and $\vec{C_2}$ are

$$\vec{C_1} = (I - \delta)^{-1}\Phi^{-1}\vec{P_0}, \tag{9a}$$

$$\vec{C_2} = -D^{-1}(L)\delta\vec{C_1}, \tag{9b}$$

where

$$\delta = D(L)\left(Y_L\Phi + \Phi\Gamma\right)^{-1}\left(Y_L\Phi - \Phi\Gamma\right)D(L), \tag{10}$$

with $\Gamma_{ij} = \mathrm{j}k_i\delta_{ij}$. Note that the admittance matrix in the input plane $x = 0$ can be written as function of the output admittance matrix Y_L:

$$Y_0 = \Phi\Gamma(I + \delta)(I - \delta)^{-1}\Phi^{-1}. \tag{11}$$

A. Validation, convergence

1. Waveguide modes

In the simple case that is studied in this section, eigenmodes (α_i, ϕ_i) of the transverse eigenproblem

$$\left[\frac{1}{\tau}\frac{\partial}{\partial z}\left(\frac{1}{\tau}\frac{\partial}{\partial z}\right)\right]\phi = -\alpha^2\phi \tag{12}$$

can be calculated analytically. Eigenvalues are

$$\alpha_i^{(\text{ana.})} = \frac{i\pi}{(\tau_0 h + l)}, \qquad i \geq 0, \tag{13}$$

while associated eigenfunctions are

$$\phi_i^{(\text{ana.})}(z) = \cos\big(\alpha_i(\tau_0 z + l)\big). \tag{14}$$

Eqs. (13) and (14) provide reference solutions for a study of the validity and convergence of the finite element computation shown above. Knockaert and De Zutter showed the completeness of these eigenmodes in a parallel plate waveguide with PML termination[8].

Fig. 2(a) shows the spectrum of eigenvalues α_i, obtained both analytically (Eq. 13) and numerically (eigenvalues of $M^{-1}K$). Parameters are $l = 3$, $h = 2$ (dimensionless units), $A = 1$ and $\beta = \pi/4$, and the interval $z \in [-l, h]$ is discretized on a regular grid of 50 nodes, so that $\Delta z = z_n - z_{n-1} = 0.1$. Note that in the initial case of the semi-infinite halfspace, the spectrum of eigenvalues is a continuum corresponding to the real axis.

In the spectrum of analytical eigenvalues ('$\circ$'), we see that the PML has two visible effects. First, it rotates the continuum due to the complex stretching (App. A). Second, it discretizes the continuum due to the truncation of the PML at a finite width.

From Eq. (13) it can be easily shown that the angle $\gamma = \tan^{-1}\left(\frac{\Re\{\alpha_i\}}{\Im\{\alpha_i\}}\right)$ between the tilted straight line and the real axis is directly related to the PML parameters A and β; notably, γ tends toward $-\beta$ when the PML is infinitely wide.

The numerical spectrum ('$\times$') obtained using the FEM displays three families of eigenvalues in a typical pitchfork shape[16]. From the origin in the complex α-plane, the first eigenvalues follow the path of the analytical eigenvalues and correspond to eigenfunctions located on both the "physical" domain ($z < 0$) and the PML (Modes 1 to 4 of Fig. 2(b)). Then the spectrum splits, to display two families of eigensolutions. Eigenvalues close to the real axis correspond to eigenfunctions located mostly in the lower, "physical", part of the computational domain (Mode 18 of Fig. 2(b)), while eigenvalues below the analytical spectrum correspond to eigenfunctions located mostly in the PML (Mode 13 of Fig. 2(b)).

When the number of nodes in the mesh N increases, numerical eigenvalues converge to analytical solutions. The convergence, however, is low, with a relative error

$$\epsilon_i^{(\alpha)} = \left| \frac{\alpha_i - \alpha_i^{(\text{ana.})}}{\alpha_i^{(\text{ana.})}} \right| \times 100 \tag{15}$$

decreasing as $\simeq 1/N$ or slower (Fig. 3(a)). In the same way, the convergence of the eigenfunctions, as measured by

$$\epsilon_i^{(\phi)} = \sqrt{\frac{\int_{-l}^{h} \|\phi_i - \phi_i^{(\text{ana.})}\|^2 \,\mathrm{d}z}{\int_{-l}^{h} \|\phi_i^{(\text{ana.})}\|^2 \,\mathrm{d}z}} \times 100, \tag{16}$$

is also quite slow (Fig. 3(b)). Thus, even with a large number of nodes in the FEM mesh, very few eigenvalues

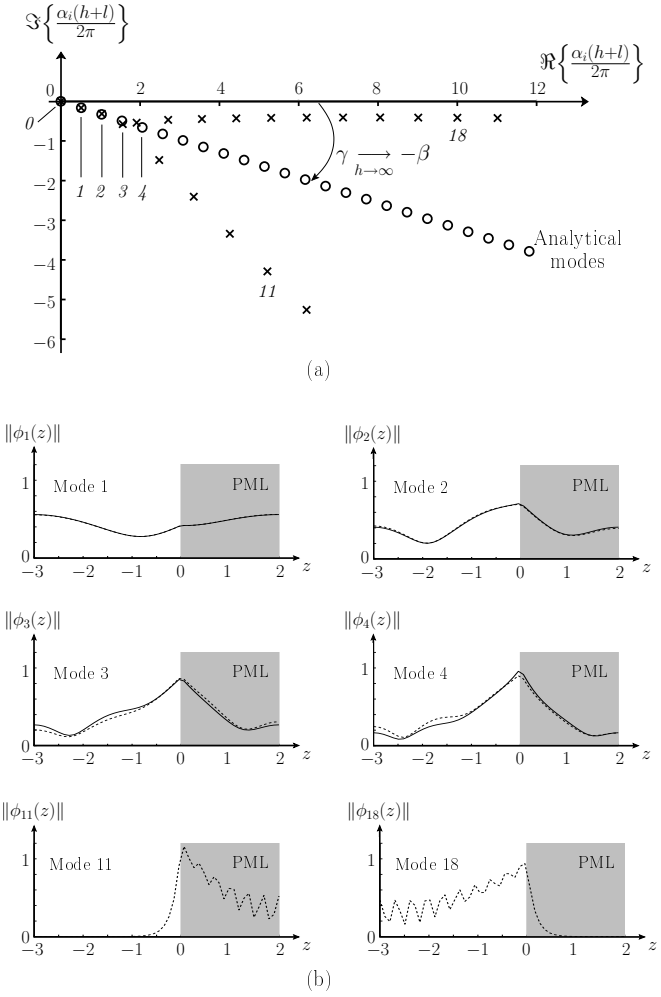

Figure 2. (a) Spectrum of the eigenvalues α_i: '$\circ$' analytical eigenvalues, '$\times$' FEM. (b) Examples of eigenfunctions, corresponding to labeled eigenvalues in the sprectrum: ('$-$') analytical eigenfunctions, ('$- - -$') FEM. Parameters are $l = 3$, $h = 2$ (dimensionless units), $A = 1$, $\beta = \pi/4$, and $N = 50$.

and eigenfunctions are accurately computed. However, in this paper, we are interested in the propagation of waves. Besides, as it will be shown in the following, using all the found modes gives the method a satisfying convergence.

2. *Computation of a pressure field*

The validity and convergence of the modal-FE method is studied in this paragraph by comparison between a reference pressure field and its computation with Eq. (7). The chosen reference field, shown in Fig. 4(a), is the solution of a "full FE" computation: the domain under study is meshed with triangular elements, with a maximum mesh size (maximum length between two nodes) $\text{mms} = \lambda/10 = 0.05$, λ the wavelength. At the input of the waveguide, the source condition is an incident gaussian beam, written as

$$P_{0n} = \exp\left(\frac{-(z_n - z_\text{s})^2}{2\sigma^2} + \mathrm{j}k\sin(\theta_z) z_n\right), \; n \geq 1, \tag{17}$$

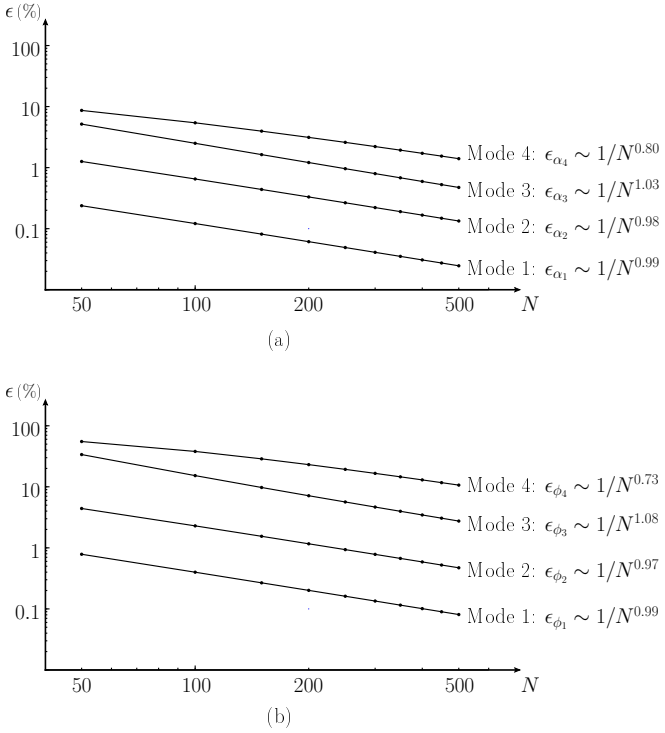

Figure 3. (a) Convergence of the four first eigenvalues when the number of nodes used in the mesh increases. (b) Convergence of the corresponding eigenfunctions.

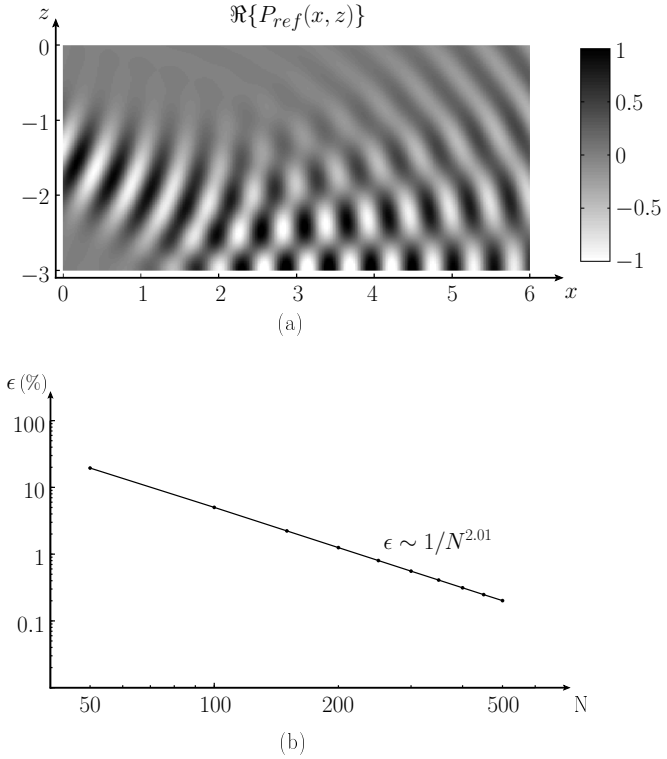

Figure 4. (a) Reference field considered to evaluate the convergence of the Modal-FE method is the "Full FE" solution of an incident gaussian beam. (b) Convergence of the modal-FE method with the number of nodes N in the cross-section $z \in [-l, h]$. In these computations, $l = 3$ (dimensionless units), $z_s = -1.5$, $\sigma = 0.4$, $\theta_z = -\pi/8$ and $k = 12.56$. PML parameters are $h = 2$, $A = 1$ and $\beta = \pi/4$.

with $z_\mathrm{s} = -1.5$ the central point of the beam, $\sigma = 0.4$ the standard deviation (related to the beam width), $\theta_z = -\pi/8$ the angle of incidence and $k = 12.56$ the wavenumber.

To compute this field using the modal-FE method, the radiation condition at the output end of the computational domain is taken as the characteristic admittance matrix Y_c that can be easily deduced from Eqs. (9) and (10) by imposing $\vec{C}_2 = \vec{0}$ (no back travelling wave downstream from the source point): $Y_\mathrm{c} = \Phi\Gamma\Phi^{-1}$.

The convergence of the solution with the number of nodes in the z-direction, as measured by

$$\epsilon = \sqrt{\frac{\int_{-l}^{0}\int_{0}^{L} \|p - p_\mathrm{ref}(x,z|x_\mathrm{s},z_\mathrm{s})\|^2 \,\mathrm{d}x\mathrm{d}z}{\int_{-l}^{0}\int_{0}^{L} \|p_\mathrm{ref}(x,z|x_\mathrm{s},z_\mathrm{s})\|^2 \,\mathrm{d}x\mathrm{d}z}} \times 100, \quad (18)$$

is relatively rapid, with an error decreasing as $1/N^2$ (Fig. 4(b)). Besides, for a reasonable number of nodes used to discretize the cross section ($N = 100$), the total error on the field is acceptable ($\epsilon = 5\%$) while only two modes are accurately obtained. This implies that the "spurious" modes (*e.g.*, modes 11 and 18 in Fig. 2(b)) play a substantial role for the convergence of the method, in addition to the "physical" ones.

B. Propagation over a ground with a piecewise constant, range dependent, height

Now that the modal-FE approach has been formulated in a uniform case - the halfplane was grounded at $z = -l$ = constant - the case of an abrupt change of the ground level, as shown in Fig. 5(a), is considered, so that problems with irregular boundaries can be studied in the following. At the discontinuity, the acoustic pressure p and the longitudinal component of its gradient, $\partial_x p$, satisfy the continuity conditions

$$\begin{cases} p^{(\mathrm{u})} = p^{(\mathrm{d})} & z \in S^{(\mathrm{u})}, \\ \partial_x p^{(\mathrm{u})} = \partial_x p^{(\mathrm{d})} & z \in S^{(\mathrm{u})}, \\ \partial_x p^{(\mathrm{d})} = 0 & z \in S^{(\mathrm{d})} \setminus S^{(\mathrm{u})} \end{cases} \quad (19)$$

where superscripts $^{(\mathrm{u})}$ and $^{(\mathrm{d})}$ denote variables associated, respectively, to the section upstream and downstream from the discontinuity. Substituting developments of p and $\partial_x p$ on the basis $\{\psi_n\}$ in Eqs. (19) straightforwardly leads to the following matricial expressions of the continuity conditions

$$\vec{P}^{(\mathrm{u})} = F\vec{P}^{(\mathrm{d})} \quad (20a)$$

$${}^{t}F\vec{Q}^{(\mathrm{u})} = Q^{(\mathrm{d})} \quad (20b)$$

for the wave field, and

$$Z^{(\mathrm{u})} = FZ^{(\mathrm{d})}\,{}^{t}F, \quad (21)$$

for the impedance matrix Z ($Z = Y^{-1}$ is the inverse of the admittance matrix defined previously). When iden-

tical FEM meshes (same node coordinates and same interpolating functions) are generated both in $S^{(\mathrm{u})}$ and $S^{(\mathrm{d})} \cap S^{(\mathrm{u})}$, the matching matrix F is simply $F_{ij} = \delta_{ij}$, δ_{ij} the Kronecker symbol.

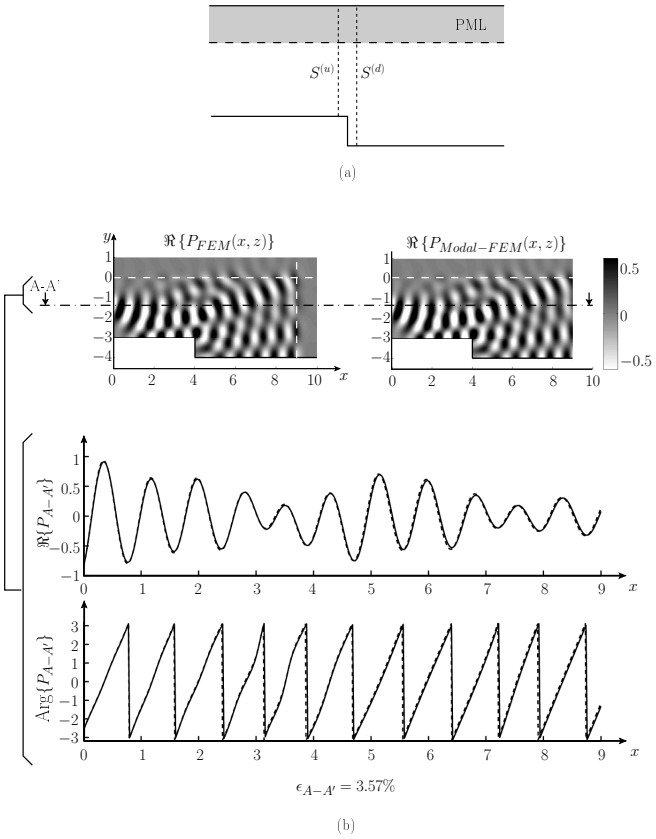

Figure 5. (a) Cross-section discontinuity. (b) Validation of the modal-FE method by a 2D FEM computation in the case of cross-section expansion.

Then, the wave field over this discontinuity can be computed, following three steps[14]:

- first, both the local waveguide modes upstream and downstream from the discontinuity are solved as described previously in the paper;
- second, given a radiation admittance or impedance at the output of the computational domain, the input admittance (or impedance) is computed by using alternatively Eqs. (11) and (21);
- third, given an input condition, the pressure field is computed down the street using alternatively Eqs. (7) in straight segments with respect to the x-axis, and Eqs. (20) at cross-section discontinuities.

Fig. 5(b) shows an example of such a computation, and the obtained pressure field is compared with the solution of a "full FE" computation. At the entrance of the waveguide, an incident gaussian beam with $z_\mathrm{s} = -1.5$, $\sigma = 0.4$, $\theta_z = -\pi/10$ and $k = 8$ (Eq. 17) is chosen as input condition. For the "full-FE" computation, the maximum mesh size of the triangular mesh is mms $= \lambda/10 = 0.0785$, and for the modal-FE computation, the discretization step in the cross-section is $\Delta z =$ mms. Both methods give very similar results. For example, on the line A-A' defined by $z =$ constant $= z_\mathrm{s}$, both the real part and the phase of the two solutions fit very well.

III. CASE OF A 3D OPEN WAVEGUIDE

In this section, the modal-FE formalism is extended to the case of 3D irregular open waveguides. Such a geometry may represent a street canyon with buildings of different sizes. As done before, PML are introduced to substitute the original, open, problem to the problem of a closed, irregular, waveguide. Following the same procedure as described in the 2D case, the pressure field is developed on a basis of interpolating polynomials $\psi_n(y,z)$: $p(x,y,z) = {}^{\mathrm{t}}\vec{\psi}\vec{P}$, and $\vec{P}$ is the solution of the matricial wave equation (5), with

$$M_{mn} = \int_S \tau \psi_m \psi_n \,\mathrm{d}y\mathrm{d}z, \tag{22a}$$

$$K_{mn} = -\int_S \frac{1}{\tau}\left(\frac{\partial\psi_m}{\partial y}\frac{\partial\psi_n}{\partial y} + \frac{\partial\psi_m}{\partial z}\frac{\partial\psi_n}{\partial z}\right)\mathrm{d}y\mathrm{d}z, \tag{22b}$$

where S denotes the cross-section.

As in the 2D case, the modal-FE method is compared with a FEM computation performed in a 3D waveguide having a sudden width expansion (Fig. 6(a)). For the FEM computation, third order interpolating polynomials are used on a tetrahedric mesh with a maximum mesh size mms $= \lambda/1.36 = 0.25$ (it leads to a ~ 72000 dof discretized problem). For the modal-FE computation, the maximal mesh size of the triangular mesh in the cross-sections is mms $= \lambda/10 = 0.034$ (~ 4800 dof). At the input of the waveguide, the source condition is an incident gaussian beam, written as

$$P_{0n} = \exp\left(\frac{-(y_n - y_\mathrm{s})^2 - (z_n - z_\mathrm{s})^2}{2\sigma^2} + \ldots \right.$$
$$\left. \mathrm{j}k[\sin(\theta_y)y_n + \sin(\theta_z)z_n]\right), \tag{23}$$

with $(y_\mathrm{s}, z_\mathrm{s}) = (0, 0.3)$ the central point of the beam, $\sigma = 0.2$ the standard deviation (related to the beam width), $\theta_y = -\pi/8$ the angle of incidence with the y-axis, $\theta_z = -\pi/15$ the angle of incidence with the z-axis and $k = 18.48$ the wavenumber. Again, the agreement between the two methods is good, with an error $\epsilon_{\text{A-A'}} \simeq 4\%$ estimated on the line A-A' (Fig. 6(b)).

An example of computation of the wave field in an irregular open waveguide, displaying a street canyon, enclosed by buildings with different sizes, is shown in Fig. 7. The mean width of the canyon is 1 in dimensionless units, with variations up to 15%. The buildings height vary from 1 to 1.9. The wavelength of the source - a gaussian beam as in previous results in the paper - is 0.3: the half-wavelength is thus of the order of size of the wall irregularities. The results clearly shows the waveguiding effect, together with the radiative losses above the street.

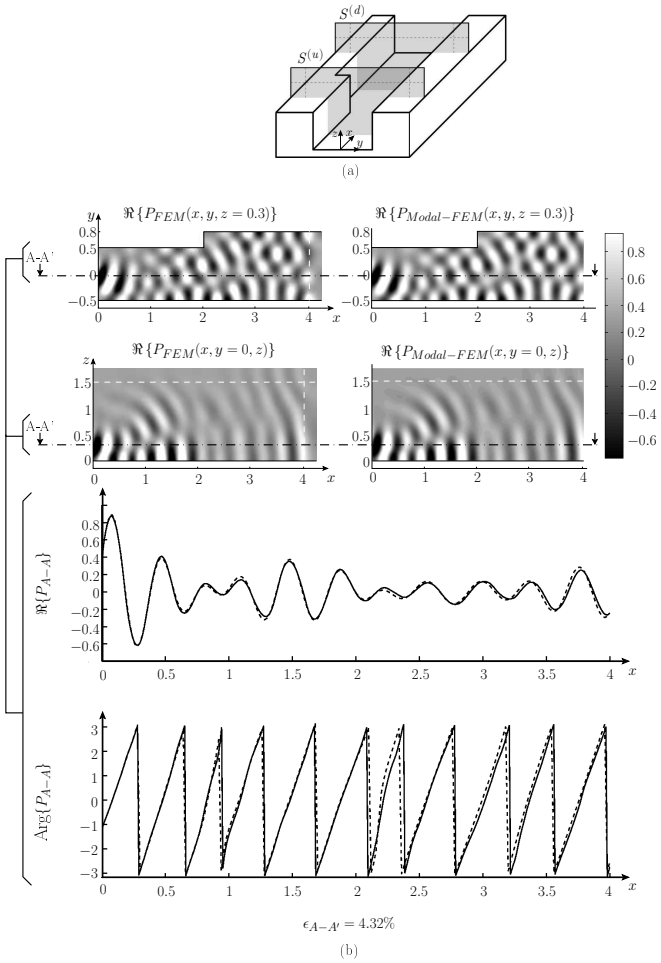

Figure 6. (a) Sudden width expansion in a 3D openfor a reasonable number of nodes used to discretize the cross section ($N = 100$), the total error on the field is acceptable ($\epsilon = 5\%$) while only two modes are accurately obtained. waveguide. (b) Validation of the modal-FE method by a 3D FEM computation in the case of a cross-section expansion, the two plots on top show real parts of the solutions on a xy-plane with $z = z_s$ and the two plots below show real parts of the solutions on a x-plane with $y = y_s$. Then, real part and phase of FEM solution (solid line) and Modal-FE solution (dashed line) are shown along the line A-A defined by $(y, z) = (y_s, z_s)$.

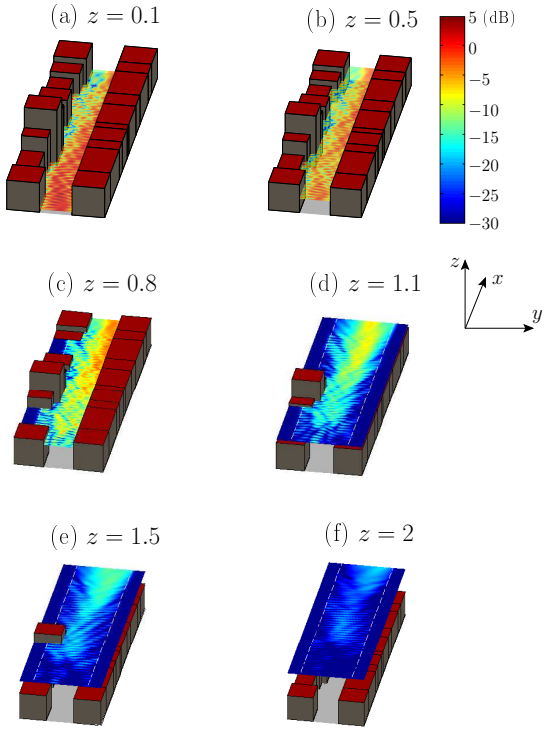

Figure 7. (color online) Example of a pressure field (modulus) in an irregular open waveguide modeling a street canyon, at six different heights. The mean width of the street is 1 (dimensionless units), with variation up to 15%, and the height of the buildings vary from 1 to 1.9. The wavelength is 0.3.

The scattering by the the façades irregularities results in a complex pattern of the pressure field.

IV. BEAT PHENOMENON BETWEEN TO PARALLEL OPEN WAVEGUIDES

As it was shown above in the paper and in previous work[15], the modes of a canyon (seen as an open waveguide) are determined as the resonances of the rectangular cross-section, l wide and $2l$ deep, open in an infinite half-space (we choose $l = 1$, dimensionless units). The mode $\phi_{(1,0)}$ (one vertical nodal line - line on which the eigenfunction is zero -, no horizontal nodal line) in Fig. 8(a) with the associated eigenvalue $\alpha_{(1,0)}l/2\pi = 0.5123 - 0.0016\mathrm{j}$ is an example of such a resonance (FEM computation). Therefore, if one consider two parallel identical canyons separated by a distance e (we choose $e = 0.3$), one can expect the global waveguiding structure to exhibit coupled eigenmodes: a resonance of the original, single, cross-section (Fig. 8(a)) will split into two distinct resonances when considering two parallel canyons. One of the resonances corresponds to a symetrical eigenmode (mode $\phi^{(\mathrm{s})}_{(1,0)}$ in Fig. 8(b) on the left, with the associated eigenvalue $\alpha^{(\mathrm{s})}_{(1,0)}l/2\pi = 0.5138 - 0.0024\mathrm{j}$), with respect to the plane of symmetry of the structure defined by $y = 0$, while the other corresponds to an antisymetrical eigenmode (mode $\phi^{(\mathrm{a})}_{(1,0)}$ in Fig. 8(b) on the right, with the associated eigenvalue $\alpha^{(\mathrm{a})}_{(1,0)}l/2\pi = 0.5118 - 0.0011\mathrm{j}$).

At the input ($x = 0$) of the two canyons structure, a source condition is considered as the combination $p_0 = \phi^{(\mathrm{s})}_{(1,0)} + \phi^{(\mathrm{a})}_{(1,0)}$. Because of the great similarity between the eigenfunctions of both the symetrical and antisymetrical modes, the wave field in one canyon shows a similar pattern as $2\phi_{(1,0)}$, while it almost vanishes in the second canyon (Fig. 8(c)). Downstream from the source plane, the field is computed by propagating the two modes of the combination:

$$p(x, y, z) = \phi^{(\mathrm{s})}_{(1,0)} e^{\mathrm{j}k^{(\mathrm{s})}x} + \phi^{(\mathrm{a})}_{(1,0)} e^{\mathrm{j}k^{(\mathrm{a})}x}, \qquad (24)$$

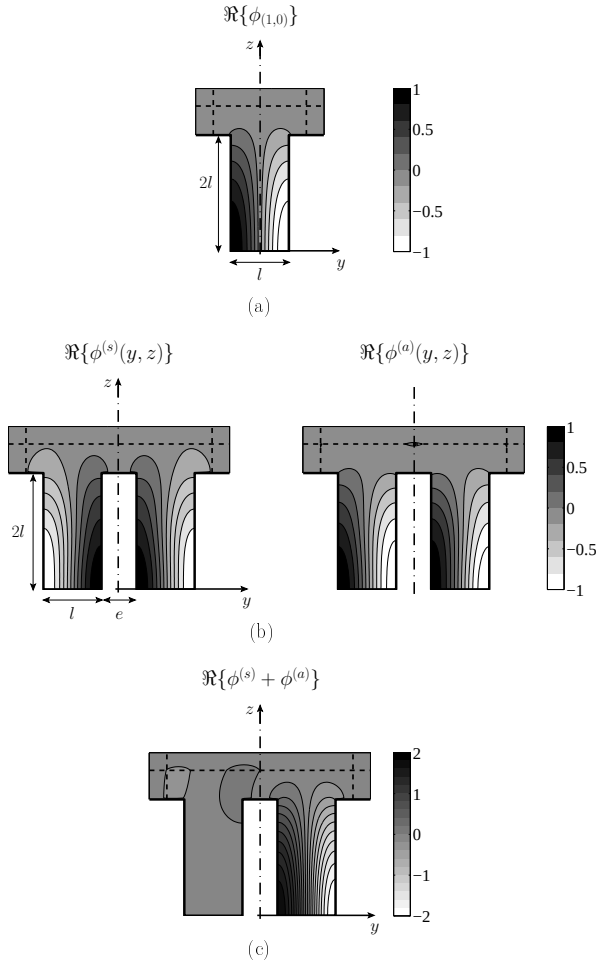

Figure 8. (a) Example of a resonance of a rectangular cavity open in an infinite halfspace (real part). The eigenmode is labelled as $(1,0)$, refering to the number of vertical and horizontal nodal lines[15] (b) Corresponding coupled eigenmodes (real part), in the case where two identical open rectangular cavities are considered. One of the modes is symmetrical (left side), while the other is antisymmetrical (right side), with respect to the plane $y = 0$. (c) The combination $p_0 = \phi^{(s)}_{(1,0)} + \phi^{(a)}_{(1,0)}$ as input condition.

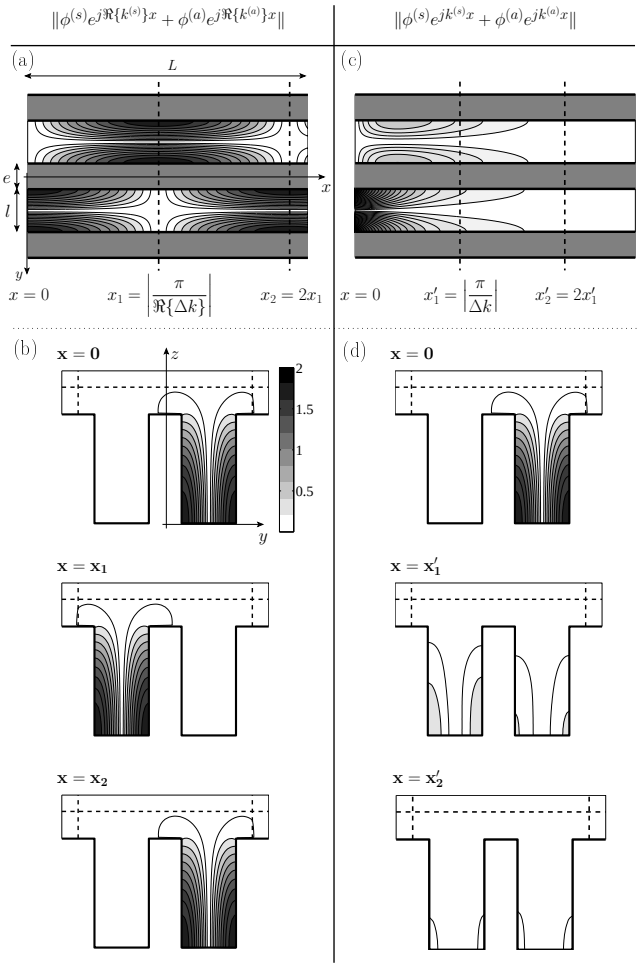

Figure 9. (a) and (b): the propagation constants $k^{(\mathrm{s})}$ and $k^{(\mathrm{a})}$ of the modes have artificially been put to zero so that the modes do not decrease exponantially. (a) Longitudinal cut at $z = l/2$ of the field (modulus) downstream from the source plane, (b) successive transversal cuts of the field (modulus) at different distance ($x = 0$, $x = x_1$, $x = 2x_1$) of the source plane. (c) and (d): exact case where the propagation constants $k^{(\mathrm{s})}$ and $k^{(\mathrm{a})}$ are complex so that the modes are leaky and lose energy while propagate along the canyons. (c) Longitudinal cut at $z = l/2$ of the field (modulus) (d) successive transversal cuts of the field (modulus) at different distance ($x = 0$, $x = x'_1$, $x = 2x'_1$).

where $k^{(\mathrm{s})} = \sqrt{k^2 - {\alpha^{(\mathrm{s})}_{(1,0)}}^2}$ and $k^{(\mathrm{a})} = \sqrt{k^2 - {\alpha^{(\mathrm{a})}_{(1,0)}}^2}$. The propagation constants $k^{(\mathrm{s})}$ and $k^{(\mathrm{a})}$ of the two modes being slightly different ($\alpha^{(\mathrm{s})}_{(1,0)}$ and $\alpha^{(\mathrm{a})}_{(1,0)}$ are very close), the modes, that originally interfere ($x = 0$) so that only one of the canyons is excited, become out of phase while propagate along the canyons, leading to an energy transfer in the second canyon, where, originally, no field was generated.

Fig. 9 gives two illustrations of this coupling between the two canyons. In Figs. 9(a) and (b), the imaginary part of the propagation constants $k^{(\mathrm{s})}$ and $k^{(\mathrm{a})}$ has been artificially put to zero so that the modes do not decrease exponentially. Fig. 9(a) show a horizontal cut of the field at a height $z = l/2$ and Fig. 9(b) shows successive vertical cuts of the field at different distance x from the source plane. At a distance $x_1 = |\pi/\Re\{\Delta k\}|$ with $\Delta k = k^{(\mathrm{s})} - k^{(\mathrm{a})}$, the two modes are in opposite phase and, as a consequence the field in the first canyon is almost zero, while it is maximum in the second one. Then, at a distance $x_2 = 2x_1$, the two modes are in phase and the field is maximum in the first canyon while it is almost zero in the second one. As the modes do not decrease while propagating, the successive energy transfers between the two canyons lead to a beat phenomenon with a space period $2x_1$.

Figs. 9(c) and (d) illustrate the exact case with complex propagation constants so that the modes are leaky and lose energy while propagating along the canyons. As a consequence, there is no more beat phenomenon, but only one significant energy transfer at a distance $x'_1 = |\pi/\Delta k|$ where the field is larger in the initial silent

canyon than in the excited one. At a distance $x'_2 = 2x'_1$, the two modes are highly damped and the field is almost zero within the two canyons.

V. ON THE EFFECT OF ABSORPTION AT THE WALLS

In the context of urban acoustics, absorption properties of buildings facades or ground surfaces must be taken into account to accurately model sound fields. A simple way to do this in the modal-FE formulation is to impose an impedance condition at the walls of the open waveguide:

$$\partial_n p = \mathrm{j}k\zeta p, \tag{25}$$

with ∂_n the normal derivative. The reduced surface admittance ζ is assumed to be locally reacting, and can vary with the frequency and position, as a function of the material it describes. In the sequel, it is assumed that the admittance does not depend on the longitudinal coordinate x, or only as a piecewise constant function, so that algebraic solutions for the impedance matrix or sound field can still be written in each uniform (*i.e.*, $\partial_x \zeta = 0$) segment.

Taking into account this new boundary condition, the wave equation in its discretized form exhibits a new term, compared to Eq. (5):

$$\vec{P}'' + \left(M^{-1}(K+Q) + k^2\right)\vec{P} = \vec{0}, \tag{26}$$

where the matrix Q is defined by

$$Q_{mn} = \mathrm{j}k \int_\Gamma \zeta \psi_m \psi_n \,\mathrm{d}\Gamma, \tag{27}$$

Γ the boundary of the cross-section. Q is a tridiagonal sparse matrix. Then, a general solution (see Eq. (7)) of Eq. (26) can be written as a function of the eigensolutions (α_i^2, ϕ_i) of the matrix $M^{-1}(K+Q)$.

To illustrate the effects of absorbing boundaries on the eigenmodes and the sound field in the waveguide, we consider in the following the canyon cross-section shown in Fig. 10. The two vertical boundaries - the façades - are splitted in two regions: the upper region, with a length h_α, has a uniform, finite, admittance, while the bottom region ($0 < z < d - h_\alpha$) is perfectly reflecting. Then the effect of varying the length h_α of the absorbing region is studied.

The dimensions of the cavity are $d = l = 1$ (dimensionless units), the frequency is chosen such that $\lambda = l/3$, and the value of the admittance is chosen as $\zeta \simeq 0.07 + 0.70\mathrm{j}$, corresponding to a weakly absorbing material. All other parameters are given in Table I.

Consider, first, the eigensolutions of $M^{-1}(K+Q)$, restricted to the resonances of the open cavity such as the indexed eigenfunctions $\phi_{(3,q)}$ with $q = 1, 2, 3$, as they were defined earlier in the paper, in the lossless case, corresponding to $h_\alpha = 0$ (For $h_\alpha > 0$, the modes are defined by continuity in the complex α-plane). Fig. 11 shows the evolution of the modulus of the three eigenfunctions when h_α increases.

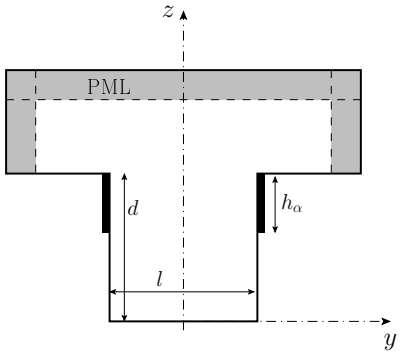

Figure 10. The vertical walls of the canyon admit two types of boundary conditions: the region below ($0 < z < d - h_\alpha$)is perfectly reflecting (homogeneous Neumann condition), while the region above ($d - h_\alpha < z < d$) has a finite admittance (Eq. (25)).

Table I. Parameters used for calculating the results in Figs. 11 and 12 (dimensionless units).

mesh		PML			gaussian beam		
mms	N	A	β	h	$(y_\mathrm{s}, z_\mathrm{s})$	σ	k
0.05	∼1400	1	$\pi/4$	0.3	$(0.15, 0.4)$	0.2	18.85

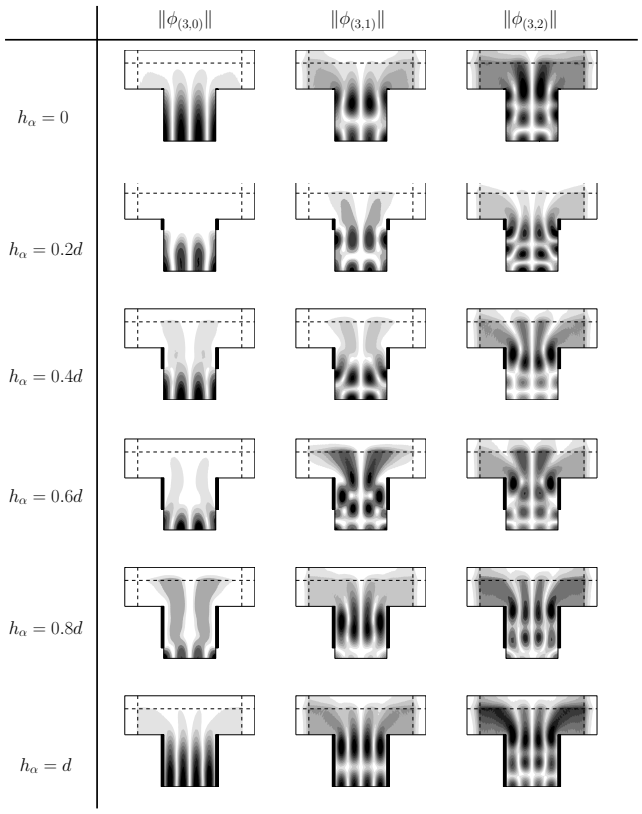

Figure 11. Evolution of three waveguide modes (modulus) with the height h_α of the absorbing part on the vertical surfaces.

When h_α is small compared with the street height d, the presence of an absorbing region at the top of the walls makes the modes more confined within the waveguide: the eigenfunctions exhibit the same global pattern, but the radiated field, above the waveguide, becomes substantially weaker. Indeed, the discontinuity of impedance at $z = d - h_\alpha$, induced by the absorbing material, enhances the effect of the geometrical discontinuity at $z = d$.

When h_α increases, the effect of increasing confinement of the modes still occurs, but then fades in favor of a new spatial distribution of the modes: the eigenfunctions $\phi_{(p,q)}$, first weakly perturbed by the small absorbing region, gradually evolve to the modes of the problem with the whole vertical boundary having a finite admittance ($h_\alpha = d$). The confinement of these new modes looks similar to the confinement of the original modes; at least there is no more visible effect of enhanced confinement.

Furthermore, Fig. 11 shows that the transition from a perturbed, confined, "rigid" mode to the corresponding "lossy" mode observed when $h_\alpha = d$ occurs later, that is, for larger values of h_α, when the order q of the mode is lower. The effect of enhanced confinement due to the absorbing region is thus stronger for the lower order modes, that are already more confined in the inital state.[15]

To deepen the qualitative observations made on the waveguide modes, consider now the influence of h_α on the whole pressure field within the canyon. The canyon is assumed to be uniform (ζ = constant) and infinitly long, and the field is generated by an incident gaussian beam (the beam parameters are in Table I). Six different configurations, from $h_\alpha = 0$ to $h_\alpha = d$, are compared through the decay of the energy flux along the canyon

$$W(x) = \frac{1}{S}\int_S \frac{1}{2}\Re\{p\vec{v}^*\}\,\mathrm{d}\vec{S} \tag{28}$$

with $S = ld$ the cross-section area of the canyon and $\mathrm{d}\vec{S} = \mathrm{d}y\mathrm{d}z\vec{e}_x$ (Fig. 12).

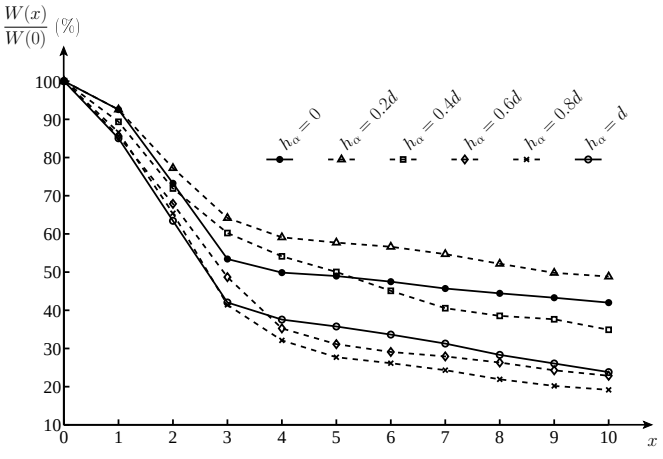

Figure 12. Decay of the energy flux along the guide as measured by the ratio $W(x)/W(x = 0)$, for different heights h_α of the absorbing part of the vertical walls.

Consider first the case of perfectly reflecting walls ($h_\alpha = 0$). As expected, the radiation in the free space above the canyon result in a monotonous decrease of the energy flux as the wave propagates. The apparent double decay of the curve can be explained by the decrease and vanishing of most of the leaky modes in the "near" field ($x < 3$) and the slower decrease of the few remaining modes, as was described in a previous study by the authors.[15]

As seen before, an absorbing material at the top of the walls may induce an effect of enhanced confinement of the modes, and then contribute to reduce the radiative losses. On the other hand, the absorbing material also induces a dissipation of the wavefield, in addition to the radiative losses. The results in Fig. 12 shows that varying h_α changes the relative importance of these two competitive effects. When h_α is small compared with d, the effect of confinement is strong enough (see discussion of Fig. 11) to prevail over the effect of absorption by the material. Thus, the energy decay along the street is slower (curve corresponding to $h_\alpha = 0.2d$ in Fig. 12). When h_α increases, the effect of absorption becomes more and more prominant. Notably, for $h_\alpha = 0.8d$, at $x = 10$, a gap of about 20% with the initial case $h_\alpha = 0$ is observed. The limit case $h_\alpha = d$ corresponds to a new spectrum of modes compared with the initial case, and the decrease of the energy flux no longer follows the trend described above. In this limit case, the interpretation is less straightforward, since the effects of localization by the geometry itself and the attenuation by absorbing walls interact in a complex way.

VI. CONCLUSION

A coupled modal-FE method has been proposed in this paper to solve the three-dimensional Helmholtz equation in an open waveguide with a discontinuously varying cross-section, chosen as an idealized model for a street canyon. It was shown that, using perfectly matched layers to turn the originally open configuration to a closed waveguiding structure, a multimodal formulation, similar to that extensively used in "classical" waveguides, can be developed, that allows a computation of the acoustic field in complex geometries of street canyons. As FEM computations are only used in the 2D cross-section, while the solution in the axial direction involves only simple matrix operations, the proposed approach is not computationally expensive. Moreover, to treat realistic urban cases, both geometrical irregularities and non uniform boundary conditions at the walls of each local cross-section can be straightforwardly taken into account in FEM computations. Besides, it was shown in a previous study that, far enough from any source or scatterer, a small number of the leaky modes propagating in the open waveguide may be sufficient to accurately model the wave field; the numerical efficiency of the present method could then be improved by an appropriate reduction of the modal basis.

Aknowledgement

This work has received support from the National French Agency for Research reference (reference of the project: ANR-JCJC-3019-01)

Appendix A: ON PERFECTLY MATCHED LAYERS (PML)

Consider the propagation of acoustic waves, solutions of the Helmholtz equation

$$\left(\Delta + k^2\right) p = f(x, y) \tag{A1}$$

in the infinite plane $(x, y) \in \mathbb{R}^2$, where all sources or scatterers, described by $f(x, y)$, are assumed to be located in the lower halfspace $y < 0$. To solve numerically Eq. (A1), a restricted computational domain has to be defined by truncating the initial infinite domain with artificial non-reflecting boundary above the region of interest.

A solution consists of introducing a layer with thickness h (for example, in region $y \in [0, h]$), in which the wave equation is modified so that outgoing waves are damped while propagating in the layer, and are of negligible amplitude at the outer boundary of the layer. Moreover, the layer must be *perfectly matched* with the physical domain of interest, that is, no reflection of waves should be generated at the interface ($y = 0$). This is done by applying a complex coordinate streching on the space variable y:

$$y \to \tilde{y} = \int_{-1}^{y} \tau(y')\, \mathrm{d}y', \tag{A2}$$

with τ a complex scalar function fulfilling

- $\Re\{\tau\}\Im\{\tau\} > 0$, in the PML domain
- $\tau(y \leq 0) = 1$, in the physical domain.

In practice, τ can be chosen as a constant function in the PML. In this paper, it is chosen $\tau = \tau_0 = \text{constant} = A\exp(\mathrm{j}\beta)$, with $A > 0$ and $\beta \in]0, \pi/2[$. Then, the wave equation to be solved is

$$\left(\frac{\partial^2}{\partial x^2} + \frac{\partial^2}{\partial \tilde{y}^2} + k^2\right) p = f(x, \tilde{y}). \tag{A3}$$

Applying the complex coordinate streching (A2) is equivalent to the substitution

$$\frac{\partial}{\partial \tilde{y}} \to \frac{1}{\tau}\frac{\partial}{\partial y} \tag{A4}$$

on the derivative with respect to y, so that the wave equation is written

$$\left(\frac{\partial^2}{\partial x^2} + \frac{1}{\tau}\frac{\partial}{\partial y}\left(\frac{1}{\tau}\frac{\partial}{\partial y}\right) + k^2\right) p = 0. \tag{A5}$$

[1] J.-P. Bérenger. A perfectly matched layer for the absorption of electromagnetics waves. *J. Comp. Phys.*, 114(2):185–200, 1994.

[2] W. P. Bi, V. Pagneux, D. Lafarge, and Y. Aurégan. Modelling of sound propagation in a non-uniform lined duct using a multi-modal propagation method. *J. Sound Vib.*, 289:1091–1111, 2006.

[3] A.-S. Bonnet-Ben Dhia, B. Goursaud, C. Hazard, and A. Prieto. Finite element computation of leaky modes in stratified waveguides. In A. Léger and M. Deschamps, editors, *Ultrasonic wave propagation in non homogeneous media*, volume 128, pages 73–86. Springer berlin Heidelberg, 2009.

[4] H. Derudder and F. Olyslager. An efficient series expansion for the 2-D Green's function of a microstrip substrate using perfectly matched layers. *IEEE Microwave Guided Wave Lett.*, 9(12):505–507, 1999.

[5] S. Félix and V. Pagneux. Sound attenuation in lined bends. *J. Acoust. Soc. Am.*, 116(4):1921–1931, 2004.

[6] G. Guillaume and J. Picaut. Implementation of complex impedance conditions and absorbing layers into a transmission line matrix model for urban acoustics applications. In *Proceedings of Euronoise'09*, 2009.

[7] M. Hornikx and J. Forrsén. The 2.5-dimensional equivalent sources method for directly exposed and shielded urban canyons. *J. Acoust. Soc. Am.*, 122(5):2532–2541, 2007.

[8] L. Knockaert and D. De Zutter. On the completeness of eigenmodes in a parallel plate waveguide with a perfectly matched layer termination. *IEEE Transactions on microwaves theory and techniques*, 50:1650–1653, 2002.

[9] T. Le Pollès, J. Picaut, M. Bérengier, and C. Bardos. Sound field modeling in a street canyon with partially diffusely reflecting boundaries by the transport theory. *J. Acoust. Soc. Am.*, 116(5):2969–2983, 2004.

[10] T. Le Pollès, J. Picaut, S. Colle, M. Bérengier, and C. Bardos. Sound-field modeling in architectural acoustics by a transport theory: Application to street canyons. *Phys. Rev. E*, 72(4):046609, 2005.

[11] K. M. Li and C. Y. C. Lai. A note on noise propagation in street canyons. *J. Acoust. Soc. Am.*, 126(2):644–655, 2009.

[12] K. K. Lu and K. M. Li. The propagation of sound in narrow street canyons. *J. Acoust. Soc. Am.*, 112:537, 2002.

[13] M. Ögren and W. Kropp. Road traffic noise propagation between two dimensional city canyons using an equivalent sources approach. *Acta Acustica united with Acustica*, 90:293–300, 2004.

[14] V. Pagneux, N. Amir, and J. Kergomard. A study of wave propagation in varying cross-section waveguides by modal decomposition. part I. theory and validation. *J. Acoust. Soc. Am.*, 100(4):2034–2048, 1996.

[15] A. Pelat, S. Félix, and V. Pagneux. On the use of leaky modes in open waveguides for the sound propagation modeling in street canyons. *J. Acoust. Soc. Am.*, 126(6):2864–2872, 2009.

[16] B. Reps and W. Vanroose. Preconditioning the Helmholtz equation with complex rotated domains. In *Proceedings of Waves 2009*, 2009.

[17] T. Van Renterghem, E. Salomons, and D. Botteldooren. Parameter study of sound propagation between city canyons with a coupled FDTD-PE model. *Appl. Acoust.*, 67:487–510, 2006.

[18] C. Vassallo. *Optical waveguide concepts, Chap. 3.* Elsevier, Amsterdam, 1991.